Journal of Nuclear and Radiochemical Sciences, Vol. 19, pp. 14-19, 2019

Articles

Mössbauer study of iron oxide nanoparticles produced by laser ablation of metallic iron in water and effects of subsequent laser irradiation

Shota Amagasa and Yasuhiro Yamada*

Department of Chemistry, Tokyo University of Science, Kagurazaka, Shinjuku-ku, Tokyo 162-8601 Japan

Received November 3, 2019; Accepted November 15, 2019; Published online November 27, 2019

Laser ablation of a metallic iron block in a flow of water was performed to produce both iron and iron oxide nanoparticles. The X-ray diffraction patterns and Mössbauer spectra for the particles indicated that the resulting material consisted of α-Fe and $Fe_{0.89}O$ nanoparticles. Transmission microscopy images demonstrated that these particles were spherical with diameters in the range of 5 to 45 nm with an average size of 20 nm. The particles were re-suspended in water and irradiated with laser light, following which the particle size was decreased and the material was further oxidized to amorphous Fe_2O_3. These results establish that laser ablation and laser irradiation have different effects when processing iron and iron oxide particles.

1. Introduction

Laser ablation in liquid (LAL) is a very useful, conventional means of producing metal particles. While the wet chemical synthesis of nanoparticles typically requires numerous chemical reagents and complicated handling processes, LAL provides a very simple method of generating nanoparticles while reducing the amount of reagents.[1] Furthermore, so-called naked nanoparticles without coating materials can be obtained using LAL, which provides a facile approach to studying the properties of such materials. Laser-based synthesis and processing have been studied extensively, as has the LAL process itself. Both fragmentation and melting resulted from laser irradiation (LI) of particles suspended in liquid have been found to be important.[2] Laser ablation (LA) of a metal has been shown to produce a plasma vapor that is rapidly quenched by the surrounding solvent to produce particles. In the case that the surrounding solvent is itself decomposed by the plasma vapor, the subsequent reactions can produce particles of various metal compounds. The chemical composition and structure of these nanoparticles can be controlled by tuning the LA conditions and varying the solvent.[3] In addition, in the case that LA is performed in a stagnant solvent, the resulting particles can be said to undergo LI. LI increases the temperature of particles, and the fragmentation and melting of the particles change their chemical composition or their shapes.

Using this LAL technique, it is possible to produce metastable materials, and our own group has demonstrated the generation of metastable copper oxide particles (Cu_4O_3) by LA in water.[4] We have also reported the reaction of iron in organic solvents to produce iron carbide particles. The LA of iron in alcohols gave α-Fe, γ-Fe, Fe_3C and amorphous iron carbides.[5] Using this technique in conjunction with a solvent flow allowed separation and collection of the different nanoparticles immediately after production, preventing further photochemical reactions of the material. The effect of LI on iron carbide nanoparticles produced by LA has also been studied,[6] and has been shown to increase the particle size and to change the composition to pure Fe_3C.

The LA of iron in various liquids has been examined.[7,8] The formation of α-Fe particles via LA of iron in water has been investigated,[9] with the surfaces of the α-Fe particles protected by surface-stabilizing reagents. The fabrication of FeO nanoparticles based on LA of a pure iron plate in poly (vinylpyrrolidone) solutions has also been reported, during which the particle size was controlled by varying the surfactant concentration.[10] Generally, LA of metallic iron in water without an adequate supply of surfactant produces iron oxide particles. It has been proposed that the LA process generates Fe clusters that react with adjacent H_2O molecules to form $Fe(OH)_2$ nanoparticles, which subsequently decompose to FeO nanoparticles at high temperature and pressure. In other work, iron oxide nanoparticles consisting of a mixture of hematite and magnetite were obtained by LA of metallic iron in water.[11] The size of such iron oxide nanoparticles can evidently be controlled by applying LI,[12] although Mössbauer spectra of the particles were not obtained in previous studies.

In the present study, LA of metallic iron in flowing water was performed to produce LA particles that were then further modified by LI in water. These LA and LI processes were analyzed separately to better understand the LAL mechanism.

2. Experimental

The experimental setups employed in this study was almost the same as those described in our previous paper.[5] Briefly, an airtight vessel attached to a cellulose acetate filter (pore size: 3.00 μm) and a diaphragm pump was employed to perform LAL. The water (200 mL) used in this process was degassed before use. An ^{57}Fe-enriched (96%) iron block ($6 \times 5 \times 1$ mm^3) was placed in the water and the vessel headspace was filled with Ar to eliminate contact with air. The vessel was maintained at atmospheric pressure. Light (532 nm, 10 Hz, 100 mJ·pulse^{-1}, beam diameter of 6 mm) from a Nd:YAG laser (Continuum, Surelite I-10) attached to a second harmonic generator was employed to perform LA. The laser pulses were introduced through a convex lens directly attached to the glass vessel and the water flow was maintained at a continual rate of 250 mL min^{-1}. The nanoparticles collected on the filter were dried in a flow of Ar.

To study the effect of LI, the LA particles were re-suspended in water in a glass vial open to the ambient atmosphere and subsequently irradiated with non-focused laser light (fluence: 350 mJ·cm^{-2}·pulse^{-1}) for 10000 pulses. The water was stirred continuously to avoid precipitation of the particles. The resulting LI particles were collected by centrifugation and fil-

*Corresponding author. E-mail: yyasu@rs.kagu.tus.ac.jp
Fax.+81-3-5261-4631

Published on Web 11/27/2019

tration.

The LA and LI particles were assessed using Mössbauer spectroscopy (Wissel, MDU1200, ^{57}Co/Rh source), X-ray diffraction (XRD; Rigaku, RINT2500, Cu-Kα) and transmission electron microscopy (TEM; JEOL, JEM-2100).

3. Results and discussion

3.1. LA particles. XRD patterns for the LA particles were acquired (Figure 1) and these patterns could be assigned to a combination of α-Fe metal (PDF#006-0696) and Wüstite FeO (PDF#01-089-0687). The diameters of the α-Fe and FeO particles were estimated using Scherrer's equation, based on the widths of the XRD peaks, to be 30 and 26 nm, respectively. A TEM image of the LA particles is provided in Figure 2. These

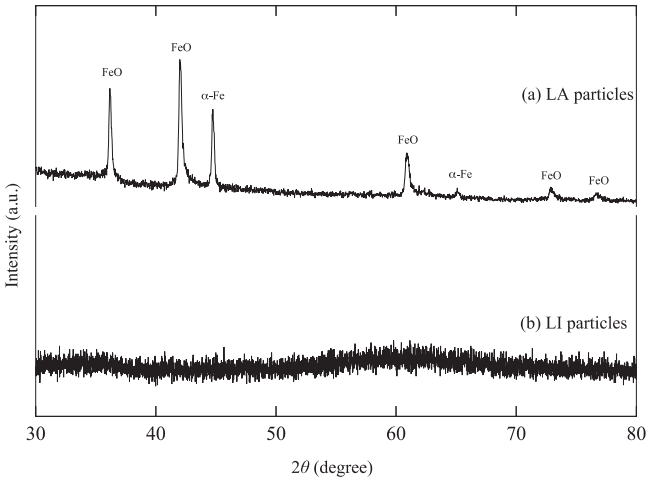

Figure 1. XRD patterns for (a) LA particles and (b) LI particles produced in water.

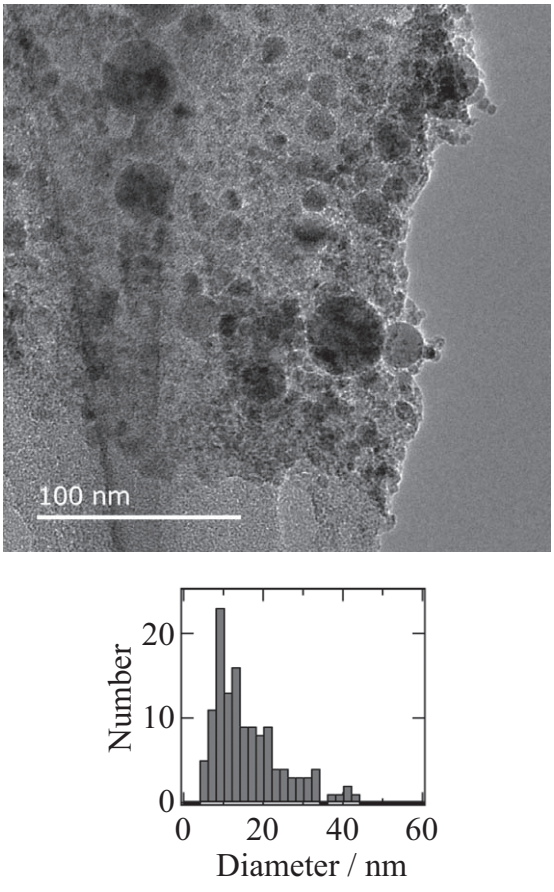

Figure 2. TEM image of LA particles and particle diameter distribution. The diameters of 129 spherical particles in the TEM image were measured to show the histogram.

particles were evidently spherical having a distribution of diameters in the range of 5 to 45 nm, with an average size of 20 nm. This result was in agreement with the diameters estimated from the XRD patterns. However, it was not possible to distinguish α-Fe and FeO in the TEM images.

Mössbauer spectra of the LA particles were obtained at temperatures from 3 to 293 K (Figure 3), and the resulting Mössbauer parameters are summarized in Table 1. The spectrum acquired at 293 K (Figure 3g) was fitted to give a combination of a sextet, a doublet and a singlet. The Mössbauer parameters for the sextet were those for α-Fe, while the doublet and the singlet were assigned to Fe^{2+} and Fe^{3+} species, respectively, in iron oxide particles. As only α-Fe and FeO were identified based on the XRD patterns for the samples without Fe^{3+} species, the Fe^{3+} indicated by the Mössbauer spectrum is believed to have been associated with defects in the FeO lattice structure. The highly energetic Fe atoms produced by LA reacted with the surrounding water molecules to generate iron oxide particles in addition to α-Fe. FeO typically has a high concentration of defects, while Fe^{2+} has both bulk Oh and defect-associated positions. Therefore the Fe^{2+} in the FeO produced a doublet at room temperature.

The same sample was examined at lower temperatures and the Fe^{2+} doublet was found to become broader at 200 K (Figure 3f), while magnetic components appeared below 100 K (Figures 3a, b, c, d and e). Wüstite Fe_xO is known to become antiferromagnetic below approximately 195 K. This value

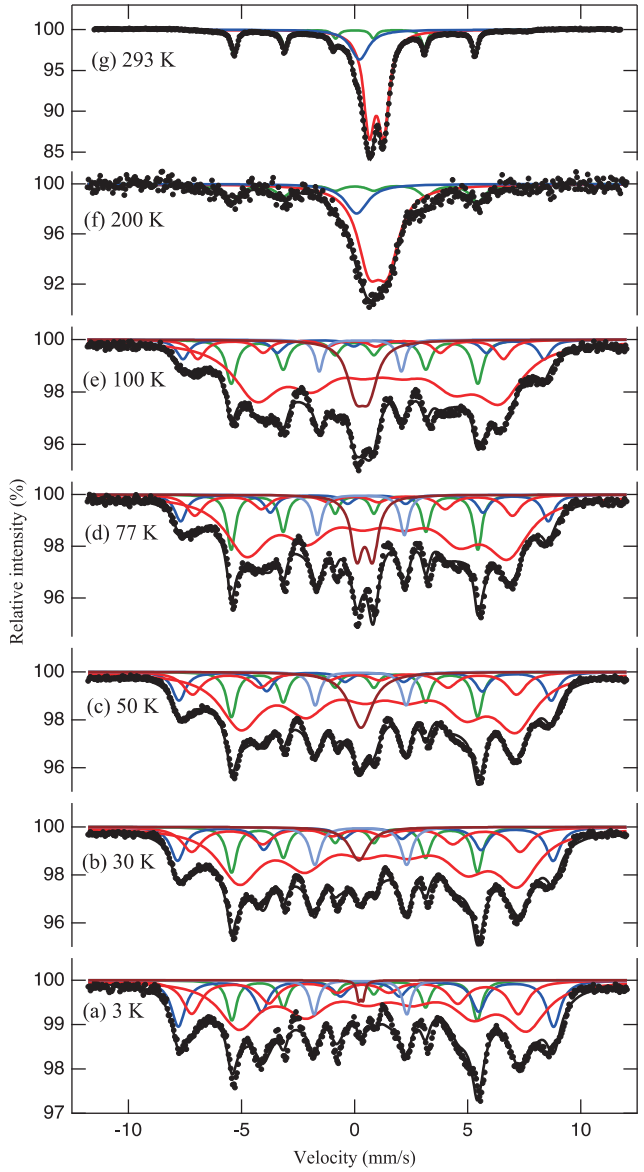

Figure 3. Mössbauer spectra of the LA particles.

TABLE 1: Mössbauer parameters of the LA nanoparticles shown in Figure 3.

Temp.	shape	species/sites	δ mm/s	ΔE_Q mm/s	H T	Γ mm/s	Area %
293 K	Sextet	α-Fe*	0	0	33.0(0)	0.33(1)	20(1)
	Doublet	Fe^{2+}	0.96(0)	0.64(0)	–	0.59(1)	64(1)
	Singlet	Fe^{3+}	0.21(1)	–	–	0.95(3)	16(1)
200 K	Sextet	α-Fe*	0	0	33.7(2)	0.81(8)	21(4)
	Doublet	Fe^{2+}	1.05(5)	0.83(4)	–	1.23(6)	65(7)
	Singlet	Fe^{3+}	0.09(7)	–	–	1.21(14)	14(6)
100 K	Sextet	α-Fe*	0	0	33.8(1)	0.56(4)	12(1)
	Sextet	Fe^{3+}/ O_h	0.81(2)	0.81(5)	49.5(2)	0.66(9)	6(1)
	Sextet	Fe^{2+}/Def. O_h	–0.15(28)	0.05(5)	41.9(2)	0.76(9)	7(1)
	Sextet	Fe^{2+}/Bulk O_h	1.14(3)	0.20(3)	33.4(2)	2.44(11)	64(4)
	Doublet	Fe^{3+}/Int. T_d	0.26(1)	3.64(2)	–	0.43(4)	1(0)
	Doublet	Fe^{3+}	0.35(1)	0.58(3)	–	0.91(6)	11(1)
77 K	Sextet	α-Fe*	0	0	33.78(6)	0.44(3)	12(1)
	Sextet	Fe^{3+}/ O_h	0.80(2)	0.54(4)	50.4(2)	0.62(8)	8(2)
	Sextet	Fe^{2+}/Def. O_h	–0.05(4)	–0.02(7)	43.5(2)	0.88(13)	9(2)
	Sextet	Fe^{2+}/Bulk O_h	1.13(3)	0.25(4)	35.8(2)	2.24(12)	59(5)
	Doublet	Fe^{3+}/Int. T_d	0.28(1)	3.85(3)	–	0.46(4)	4(1)
	Doublet	Fe^{3+}	0.45(1)	0.69(2)	–	0.62(4)	9(1)
50 K	Sextet	α-Fe*	0	0	33.7(6)	0.52(3)	12(1)
	Sextet	Fe^{3+}/ O_h	0.67(2)	0.41(3)	51.0(1)	0.70(6)	10(1)
	Sextet	Fe^{2+}/Def. O_h	–0.01(3)	–0.02(6)	44.4(2)	1.00(10)	11(2)
	Sextet	Fe^{2+}/Bulk O_h	1.22(3)	0.33(3)	37.6(2)	2.15(8)	55(3)
	Doublet	Fe^{3+}/Int. T_d	0.27(1)	4.02(2)	–	0.49(4)	4(1)
	Singlet	Fe^{3+}	0.28(2)	–	–	1.23(6)	8(1)
30 K	Sextet	α-Fe*	0	0	33.7(7)	0.52(3)	11(1)
	Sextet	Fe^{3+}/ O_h	0.63(2)	0.32(3)	51.4(1)	0.73(6)	12(2)
	Sextet	Fe^{2+}/Def. O_h	0.10(3)	0.08(7)	45.0(2)	1.11(11)	13(2)
	Sextet	Fe^{2+}/Bulk O_h	1.22(3)	0.33(3)	38.1(2)	2.19(9)	55(4)
	Doublet	Fe^{3+}/Int. T_d	0.27(1)	4.06(3)	–	0.57(4)	5(1)
	Singlet	Fe^{3+}	0.19(3)	–	–	1.01(9)	4(1)
3 K	Sextet	α-Fe*	0	0	33.6(1)	0.50(4)	11(2)
	Sextet	Fe^{3+}/ O_h	0.60(12)	0.18(3)	51.4(1)	0.74(6)	18(2)
	Sextet	Fe^{2+}/Def. O_h	0.20(2)	0.36(5)	44.7(2)	0.74(6)	17(3)
	Sextet	Fe^{2+}/Bulk O_h	1.40(5)	0.31(5)	39.4(3)	2.08(11)	49(5)
	Doublet	Fe^{3+}/Int. T_d	0.26(2)	4.10(3)	–	0.45(5)	4(1)
	Singlet	Fe^{3+}	0.28(2)	–	–	0.29(6)	1(1)

* The δ and ΔE_Q values of α-Fe were fixed to zero in the fitting procedure.

represents the Néel temperature (T_N) for this material, which will vary depending on the value of x.[13] The structure of the Mössbauer spectra acquired in this study were in agreement with this magnetic character of Fe_xO. Fe_xO exhibits a non-zero ΔE_Q because it contains defects. The Mössbauer spectrum of FeO also comprises a combination of sextets reflecting the different Fe sites produced by defects. The Mössbauer spectra of these compounds have been studied extensively and reported in the literature.[14] The Mössbauer spectrum obtained at 3 K (Figure 3a) is highly complex and was fitted to give a combination of four sets of sextets, one doublet and one singlet. One of the sextets was assigned to α-Fe, while the remaining three sextets and the doublet were assigned to Fe_xO according to the literature.[14] The sextet having the largest hyperfine magnetic field (H = 51.4 T) was attributed to substitutional octahedral high-spin Fe^{3+}, which provided charge neutrality to the defect cluster. The sextet having the highest area intensity was assigned to bulk octahedral high-spin Fe^{2+}. The line width of this sextet was extremely broadened as a result of the variety of environments caused by defects or the large surface area of the nanoparticles. Another sextet (H = 44.7 T) was assigned to the Fe^{2+} associated with the substitutional Fe^{3+}, which was expected to produce a large hyperfine field at the Fe^{2+} sites. The doublet having a large ΔE_Q value of 4.10 mm/s was due to Fe^{3+} at tetrahedral sites. This unusual large quadrupole interaction of ca. 4.0 mm/s was also reported in the literature[14]. The low intensity Fe^{3+} singlet has not been reported in the literature, and might be associated with defects or with the surfaces of the nanoparticles, which were not highly crystalline. This component appeared as a singlet below 50 K but transitioned to a doublet at 77 and 100 K. With increasing temperature, the area of this nonmagnetic component became larger while the intensity of the peak associated with substitutional octahedral high-spin Fe^{3+} decreased. This phenomenon occurred because the substitutional octahedral high-spin Fe^{3+} in the smaller crystals had a lower blocking temperature.

The Fe^{2+}/Fe^{3+} ratio in the Fe_xO nanoparticles was estimated based on the areas of the Mössbauer spectral components acquired at low temperatures, to give a value of 3.06. Thus, the stoichiometry of the Fe_xO nanoparticles was determined to be $Fe_{0.89}O$ assuming that charge balance was produced by the coexistence of Fe^{2+} and Fe^{3+}. The Mössbauer spectra therefore indicated that the nanoparticles produced by LA in water consisted of α-Fe and $Fe_{0.89}O$, while more stable iron oxides such as hematite, Fe_2O_3, or magnetite, Fe_3O_4, were not produced.

3.2. LI particles. The LA particles described above were again suspended in water and LI was performed. The XRD pattern for the resulting LI particles (Figure 1b) contains no sharp peaks, indicating the absence of a periodic crystal lattice. TEM images of the LI particles are presented in Figure 4, and show that this material consisted of spherical iron oxide particles with a diameter of ca. 10 nm, in addition to amorphous iron oxides. The high-resolution TEM image of the spherical particles in Figure 4 shows an interplanar distance, *d*, of 0.25 nm that corresponds to the (311) lattice planes of maghemite γ-Fe_2O_3. These results demonstrate that LI decreased the size of the LA particles.

Mössbauer spectra of the LI particles are provided in Figure 5, and the parameters are summarized in Table 2. The spectrum obtained at 293 K contains a paramagnetic doublet that was assigned to Fe(III) oxide species (Figure 5e). The observed isomeric shift, δ = 0.37 mm/s, corresponds to high-spin Fe^{3+} with octahedral coordination. The spectra at 77 K and 50 K still show a doublet but these peaks are now broader because of the appearance of magnetic components (Figure 5d and c). The effect of temperature on the shape of the Mössbauer spectra likely results from magnetic relaxation, although the spectra could not be fitted assuming a single relaxation time. Because the amorphous and crystalline nanoparticles generated in this study had a distribution of relaxation times (due to variations in the size of crystalline regions), the Mössbauer spectra were fitted assuming a distribution of hyperfine magnetic fields (Figure 6). The hyperfine magnetic field distribution of the spectrum obtained at the lowest temperature of 3 K was narrow with a larger mode of H = 49 T (Figure 5a and Figure 6a). However, this value was still smaller than that for bulk maghemite (H = 51 T). The temperature dependence of the Mössbauer spectra of the present LI particles was similar to that reported for amorphous Fe_2O_3 synthesized via the thermal decomposition of Prussian Blue.[16,17] A very small portion of the Fe_2O_3 was evidently in the form of γ-Fe_2O_3 nanoparticles, although the Mössbauer spectra could not be used to differentiate between the two materials because the γ-Fe_2O_3 nanoparticles were too small. The LI particles fabricated in this study are therefore believed to have comprised both amorphous Fe_2O_3 and nanocrystalline γ-Fe_2O_3 particles.

These experimental results confirm that LI decreased the size of the particles while increasing the extent of oxidation. The mechanism by which laser light interacts with colloidal nanoparticles has been discussed on a theoretical basis in the literature.[18] We also performed similar calculations to estimate the laser fluence necessary for melting of the α-Fe and Fe_xO particles in our experiments. The basic assumption of the model is that all the energy absorbed by a particle is expended

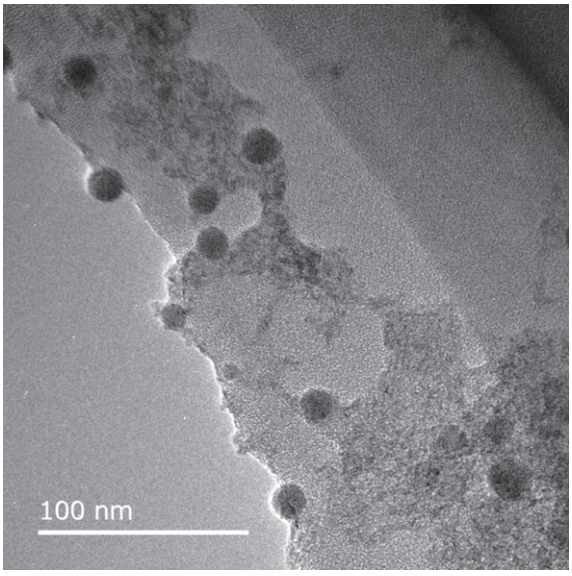

Figure 4. TEM and HR-TEM images of LI particles.

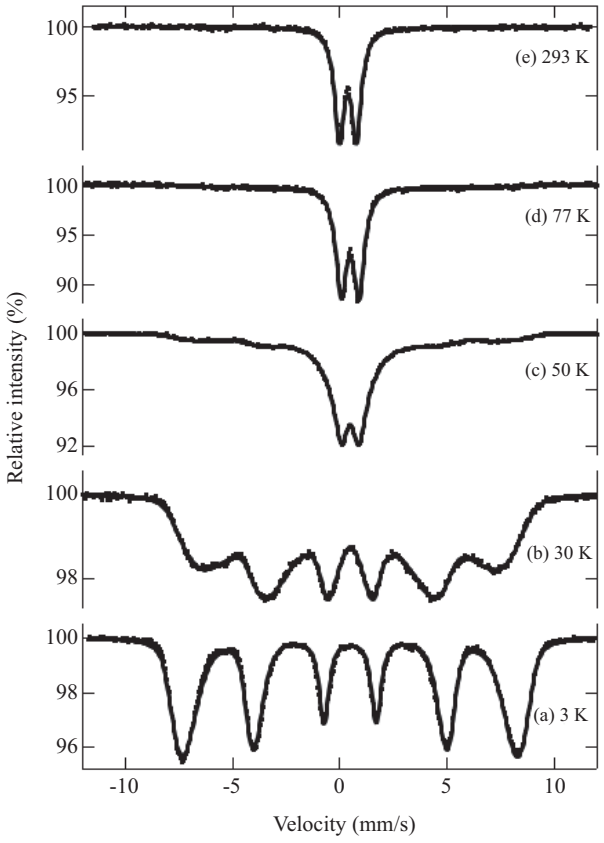

Figure 5. Mössbauer spectra of LI particles. The temperatures are shown in the figure.

TABLE 2: Mössbauer parameters for the LI amorphous particles and nanoparticles for which data are provided in Figure 5.

Temp.	δ mm/s	ΔE_Q mm/s	H^* T	Γ mm/s
293 K	0.37(1)	0.79(1)		0.54(1)
77 K	0.48(1)	0.82(1)		0.60(1)
50 K	0.48(1)	0.00(1)	4	
30 K	0.48(2)	0.00(1)	43	
3 K	0.47(1)	–0.01(1)	49	

* mode of hyperfine magnetic distribution.

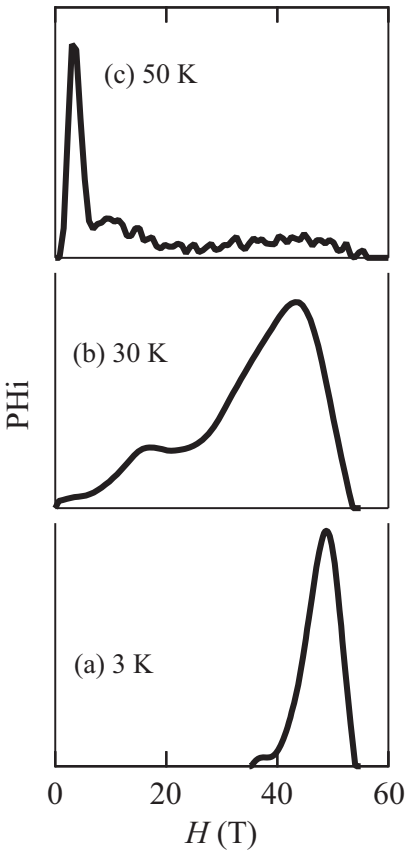

Figure 6. Hyperfine magnetic field distributions of Mössbauer spectra shown in Figure 5a, b, and c. The temperatures are shown in the figure.

in the particle heating and melting processes. The absorption efficiency, $Q_{abs}^{\lambda}(d)$, varies with the laser wavelength, λ, and particle diameter, d, and was calculated based on the Mie theory. The MiePlot v4.6 software program[19] was employed to calculate $Q_{abs}^{\lambda}(d)$, using refractive indices, n, and extinction coefficients, k, for α-Fe (n = 3.4342 and k = 3.4186) and FeO (n = 2.8882 and k = 0.50800) at λ = 532 nm previously reported in the literature.[20,21] The critical laser fluence, J, required to promote a phase transition was then determined from the equation [18,21,22]

$$J = \frac{2}{3}\rho\Delta H\frac{d}{Q_{abs}^{\lambda}(d)},$$

where ρ is the particle density and ΔH is the enthalpy required to reach the melting point (ΔH_t) or the enthalpy of melting (ΔH_m). Calculations used the following values reported in the literature:[24] α-Fe: ΔH_t = 58.645 kJ·mol^{-1} and ΔH_m = 13.807 kJ·mol^{-1}; FeO: ΔH_t = 79.081 kJ·mol^{-1} and ΔH_m = 24.058 kJ·mol^{-1}. The critical laser fluence values required to reach the melting point and to complete the melting process were calculated using these parameters (Figure 7). As the laser fluence was 350 mJ·cm^{-2}·pulse^{-1} and the particle sizes ranged from 5 to 45 nm in the present study, the calculations demonstrate that all the α-Fe and FeO particles would be expected to absorb sufficient energy (more than 30 times of the critical fluence) to melt in the water, and that these particles would also have reacted with the surrounding water molecules to oxidize. Amorphous Fe_2O_3 would have been produced by the rapid cooling of iron oxide nuclei.

4. Conclusion

The LA of metallic iron in a flow of water was found to produce both α-Fe and Fe_xO nanoparticles. These particles were spherical with an average diameter of 20 nm. Mössbauer spectra of the particles were acquired between 3 and 293 K, and the stoichiometric composition of the oxide was estimated to be $Fe_{0.89}O$. The α-Fe and $Fe_{0.89}O$ nanoparticles were subsequently re-suspended in water and irradiated with laser light (λ = 532 nm), during which they were further oxidized to amorphous Fe_2O_3 and γ-Fe_2O_3 nanoparticles. Our calculations for laser fluence indicate that the original LA particles absorbed sufficient energy to melt and to oxidize during the LI process. The results of this work confirm that LA and LI have different effects when employed for the fabrication of iron and iron oxide nanoparticles in water. In particular, LI can successfully reduce the size of nanoparticles while also promoting oxidation to form amorphous Fe_2O_3 and γ-Fe_2O_3 nanoparticles.

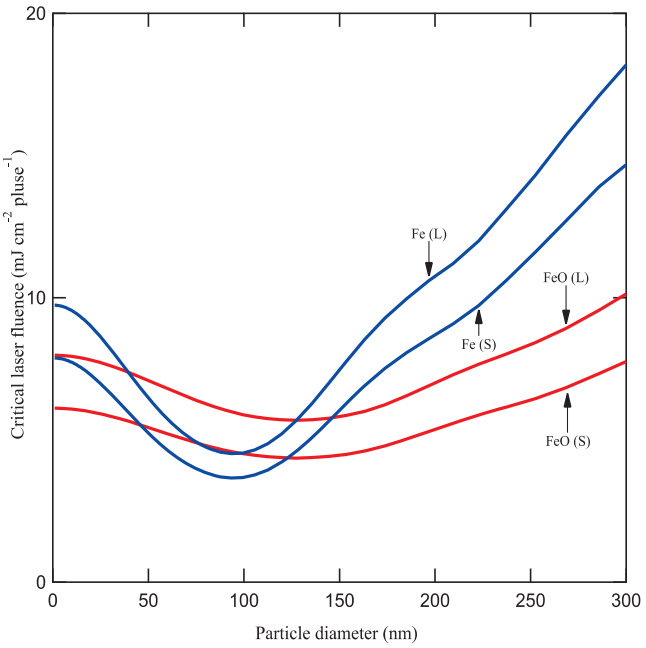

Figure 7. Calculated critical laser fluence values for melting α-Fe and FeO particles at λ = 532 nm. Legend: (Fe (S)) = heating to the melting point of Fe, (Fe (L)) = melting of Fe particles, (FeO (S)) = heating to the melting point of FeO, and (FeO (L)) = melting of FeO particles.

References

(1) H. Zeng, X. W. Du, S. C. Singh, S. A. Kulinich, S. Yang, J. He, W. Cai, *Adv. Funct. Mater. 22* (7), 1333 (2012).
(2) D. Zhang, B. Gökce, S. Barcikowski, *Chem. Rev. 117* (5), 3990 (2017).
(3) V. Amendola, M. Meneghetti, *Phys. Chem. Chem. Phys. 15* (9), 3027 (2013).
(4) K. Amikura, T. Kimura, M. Hamada, N. Yokoyama, J. Miyazaki, Y. Yamada, *Appl. Surf. Sci. 254* (21), 6976 (2008).
(5) S. Amagasa, N. Nishida, Y. Kobayashi, Y. Yamada, *Hyperfine Interact. 237*, 110 (2016).
(6) S. Amagasa, N. Nishida, Y. Kobayashi, Y. Yamada, *Hyperfine Interact. 238*, 83 (2017).
(7) A. De Bonis, T. Lovaglio, A. Galasso, A. Santagata, *Appl. Surf. Sci. 353*, 433 (2015).
(8) A. Kanitz, J. S. Hoppius, M. del Mar Sanz, M. Maicas, A. Ostendorf, E. L. Gurevich, *ChemPhysChem 18* (9), 1155 (2017).
(9) Y. Vitta, V. Piscitelli, A. Fernandez, F. Gonzalez-Jimenez, J. Castillo, *Chem. Phys. Lett. 512* (1–3), 96 (2011).
(10) P. Liu, W. Cai, H. Zeng, *J. Phys. Chem. C 112* (9), 3261 (2008).

(11) V. Amendola, M. Meneghetti, G. Granozzi, S. Agnoli, S. Polizzi, P. Riello, A. Boscaini, C. Anselmi, G. Fracasso, M. Colombatti, *J. Mater. Chem. 21* (11), 3803 (2011).
(12) V. Amendola, P. Riello, S. Polizzi, S. Fiameni, C. Innocenti, C. Sangregorio, M. Meneghetti, *J. Mater. Chem. 21* (46), 18665 (2011).
(13) F. B. Koch, M. E. Fine, *J. Appl. Phys. 38* (3), 1470 (1967).
(14) C. Wilkinson, P. D. Battle, D. A. O. Hope, A. K. Cheetham, G. J. Long, *Inorg. Chem. 23* (20), 3136 (1984).
(15) J. Hesse, A. Rübartsch, *J. Phys. E: Sci. Instrum.* 7, 526 (1974).
(16) R. Zboril, L. Machala, M. Mashlan, V. Sharma, *Cryst. Growth Des. 4* (6), 1317 (2004).
(17) L. Machala, R. Zboril, A. Gedanken, *J. Phys. Chem. B 111* (16), 4003 (2007).
(18) A. Pyatenko, H. Wang, N. Koshizaki, T. Tsuji, *Laser Photonics Rev. 7* (4), 596 (2013).
(19) P. Laven, *Appl. Optics, 42* (3), 436 (2003).
(20) W. S. M. Werner, K. Glantschnig, C. Ambrosch-Draxl, *J. Phys. Chem. Ref. Data 38* (4), 1013 (2009).
(21) Th. Henning, B. Begemann, H. Mutschke, J. Dorschner, *Astron. Astrophys. Suppl. Ser. 112*, 143 (1995).
(22) Y. Ishikawa, N. Koshizaki, A. Pyatenko, *Trans. Electron. Inf. Syst. 135* (9), 1066 (2015).
(23) A. Pyatenko, H. Wang, N. Koshizaki, *J. Phys. Chem. C 118* (8), 4495 (2014).
(24) M. W. Chase, J. L. Curnutt, H. Prophet, A. N. Syverud, L. C. Walker, *J. Phys. Chem. Ref. Data 3* (2), 311 (1974).